Intermetallics 39 (2013) 34–37

Contents lists available at SciVerse ScienceDirect

Intermetallics

journal homepage: www.elsevier.com/locate/intermet

Prediction of the morphology of $Mg_{32}(Al, Zn)_{49}$ precipitates in a Mg–Zn–Al alloy

Z.-Z. Shi [a,*], W.-Z. Zhang [b]

[a] Laboratoire d'Étude des Microstructures et de Mécanique des Matériaux (LEM3), CNRS UMR 7239, Université de Lorraine, 57045 Metz, France
[b] Key Laboratory of Advanced Materials, School of Materials Science and Engineering, Tsinghua University, Beijing 100084, China

ARTICLE INFO

Article history:
Received 11 December 2012
Received in revised form
21 February 2013
Accepted 28 February 2013
Available online 11 April 2013

Keywords:
A. Ternary alloy systems
B. Crystallography
B. Precipitates
D. Phase interfaces
F. Electron microscopy, transmission

ABSTRACT

A geometrical model has been applied to predict the morphology of faceted $Mg_{32}(Al, Zn)_{49}$ precipitates in a Mg–Zn–Al alloy using the observed orientation relationship (OR) and the lattice parameters of the precipitates and the matrix as inputs. Planes in rational or in irrational orientations with higher densities of good matching sites are more likely to be preferred, which agrees well with experimental observations.

1. Introduction

Mg–Zn is a typical age-hardenable magnesium system. Though Mg-(1.5-12)Zn (the default is wt.%) alloys are suffered to hot cracking, addition of Al can improve their castability [1]. A number of Mg–Zn–Al alloys (ZA alloy series) have been investigated with 5–14% Zn and 2–5% Al [2–9]. Because cast products account for the majority of Mg alloy usage, a large proportion of the researches on ZA alloy series are devoted to the cast alloys [2–8]. Various second phases may form in ZA alloy series, which significantly affect the performances of the alloys. Some of these phases, e.g., τ-$Mg_{32}(Al, Zn)_{49}$, are conducive to creep resistance, thereby ZA alloy series are expected to manifest superior high-temperature properties than the most common die-cast AZ91 alloy [2,10].

Wider application of Mg alloys calls for low-cost high-strength wrought Mg alloys. One of the drawbacks of commercial wrought Mg–Zn–Zr alloys (ZK alloy series) is their mild age-hardening responses by heat-treatment after wrought processes [11]. Comparatively, systematic researches on the precipitation processes of the aged ZA alloy series are sparse. Oh-ishi et al. [9] reported that addition of 3% Al to Mg-6Zn-1Mn alloy enhances its age-hardening response, though the strengthening phases remain to be Mg_4Zn_7 and $MgZn_2$. The positive effect of Al on age-hardening was also confirmed in Mg-6Zn-5Al alloy due to a dense distribution of τ-$Mg_{32}(Al, Zn)_{49}$ precipitates [12]. This paper predicts the morphology of the τ precipitates by a geometrical model using the orientation relationship (OR) between the τ phase and Mg matrix and the lattice parameters of the two phases as inputs.

2. Experimental procedures

An alloy of Mg-6Zn-5Al was prepared using high purity Mg (99.9 wt.%), Zn (99.9 wt.%) and Al (99.9 wt.%) metals by induction melting and by casting into a mild steel mold. The raw elements were supplied by General Research Institute for Nonferrous Metals in Beijing, China. The ingot was divided into several blocks, solution heat treated at 663 K (390 °C) for 48 h, quenched in water, and then aged at 453 K (180 °C) for 72 h under the protection of a tinfoil wrapping. The aging time was chosen to be long enough for the development of the τ precipitates. Specimens for transmission electron microscopy (TEM) were prepared by twin-jet electropolishing in an electrolyte consisting of 5.3 g lithium chloride, 11.16 g magnesium chlorate, 500 ml methanol and 100 ml 2-butoxy-ethanol at 223 K (−50 °C) and 15 mA. The specimens were examined in JEOL JEM-200CX operating at 200 kV.

3. Experimental results

Fig. 1a shows a TEM bright field image of an aged sample. The composite diffraction patterns of one of the precipitates marked by '1' and Mg matrix is given in Fig. 1b, in which α-Mg matrix (hexagonal close-packed (hcp), $a_\alpha = 0.31969$ nm and $c_\alpha = 0.51943$ nm

* Corresponding author. Tel.: +33 3 87547436; fax: +33 3 87315377.
E-mail address: ryansterne@sina.com (Z.-Z. Shi).

0966-9795/$ – see front matter © 2013 Elsevier Ltd. All rights reserved.
http://dx.doi.org/10.1016/j.intermet.2013.02.023

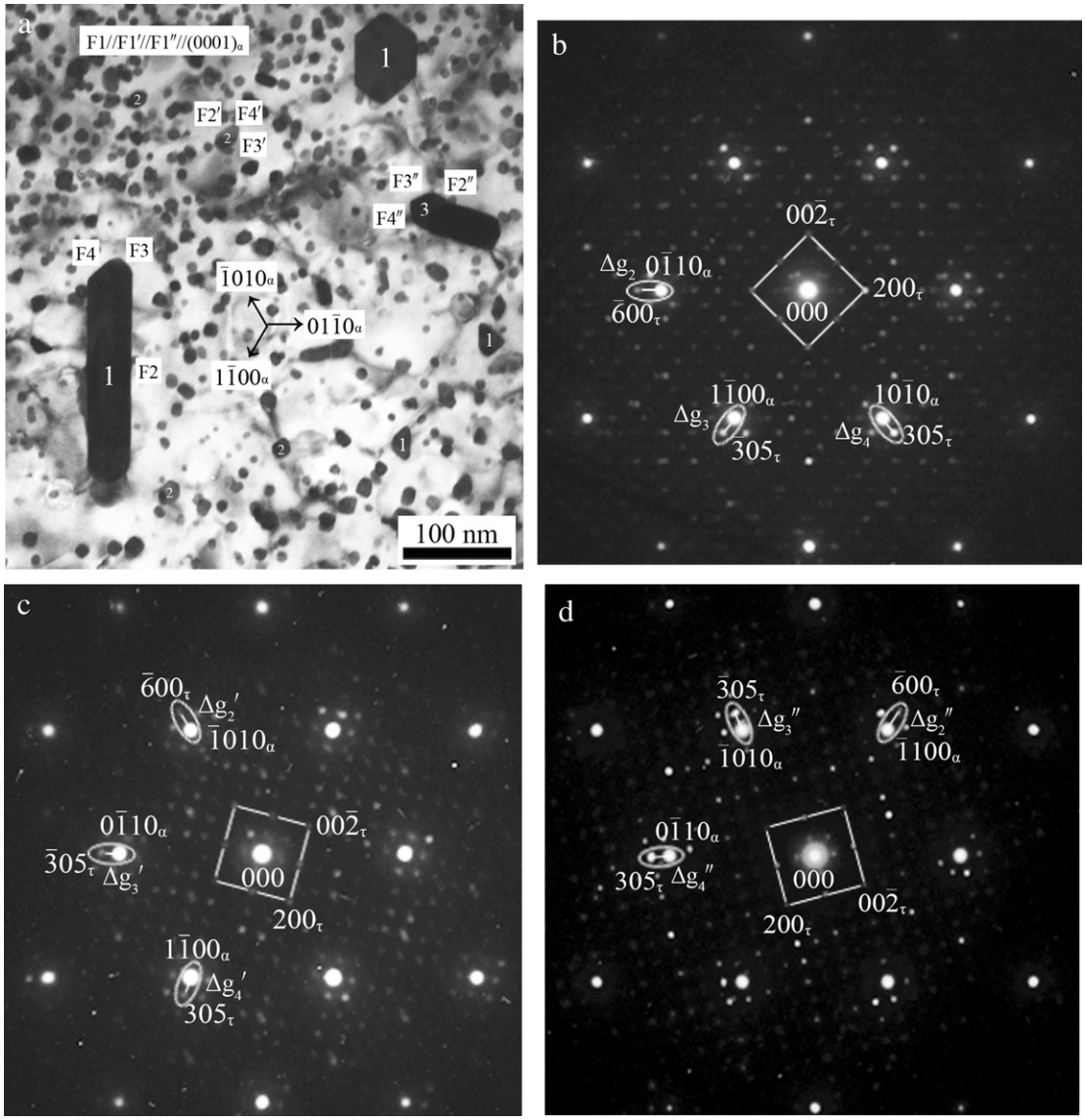

Fig. 1. (a) A TEM micrograph showing three variants (marked by 1–3, respectively) of the τ precipitates along $[0\ 0\ 0\ 1]_\alpha//[0\ 1\ 0]_\tau$ zone axis, and the corresponding composite diffraction patterns of Mg matrix and variant 1 in (b), of Mg matrix and variant 2 in (c) and of Mg matrix and variant 3 in (d).

[13]) is along $[0\ 0\ 0\ 1]_\alpha$ zone axis. Another set of the reflections can be indexed by $[0\ 1\ 0]_\tau$ zone axis of the τ phase (body-centered cubic (bcc), $a_\tau = 1.416$ nm [14]). According to Fig. 1b, the OR between the two phases can be described as $[0\ 1\ 0]_\tau//[0\ 0\ 0\ 1]_\alpha$, and $[1\ 0\ 0]_\tau//[0\ 1\ -1\ 0]_\alpha$. In the same grain, some τ phases marked by '2' or '3' in Fig. 1a show different composite diffraction patterns, which are featured by $[1\ 0\ 0]_\tau//[1\ 0\ -1\ 0]_\alpha$ or $[1\ 0\ 0]_\tau//[1\ -1\ 0\ 0]_\alpha$ in Fig. 1c and d, respectively. According to the crystal symmetries of hcp and bcc structures, precipitates '1–3' are variants of the same OR. The sizes of them vary from less than 20 nm to larger than 200 nm. Only a few large ones have been marked in Fig. 1a.

The τ precipitates usually has four facets, i.e., F1–F4 for precipitate 1, F1′–F4′ for precipitate 2, and F1″–F4″ for precipitate 3, as marked in Fig. 1a. Fi, Fi′ and Fi″ ($i = 1$–4) are crystallographically equivalent facets, which are respectively normal to $\Delta\mathbf{g}_i$, $\Delta\mathbf{g}_i'$ and $\Delta\mathbf{g}_i''$ in reciprocal space, as shown in Fig. 1b–d. The morphology of one variant can represent the crystallography of the τ phase so that the precipitate 1 is chosen to be further studied. It can be measured from Fig. 1a and b that $F1//(0\ 1\ 0)_\tau//(0\ 0\ 0\ 1)_\alpha$, $F2//(1\ 0\ 0)_\tau//(0\ 1\ -1\ 0)_\alpha$, F3 $\sim//(7\ 0\ -9)_\tau \sim//(5\ -6\ 1\ 0)_\alpha$ and F4 $\sim//(7\ 0\ 9)_\tau \sim//(5\ 1\ -6\ 0)_\alpha$. F3 and F4 are symmetrical with respect to F2. Though F1 and F2 are rational facets with low indexes, F3 and F4 are irrational facets with high indexes, which are crystallographically equivalent.

4. Morphology prediction by computer simulations

The τ phase has 162 atoms/unit-cell [14], which makes evaluating its atomic matching with α-Mg extremely complicated. However, evaluating its lattice matching with α-Mg lattice is much easier and is probably enough to reflect the interfacial structures of the preferred facets. According to the observed OR, a set of standard **x**, **y** and **z** axes are specified for further analysis, which are $\mathbf{x}//[1\ 0\ 0]_\tau//[0\ 1\ -1\ 0]_\alpha$, $\mathbf{y}//[0\ 0\ -1]_\tau//[-2\ 1\ 1\ 0]_\alpha$, and $\mathbf{z}//[0\ 1\ 0]_\tau//[0\ 0\ 0\ 1]_\alpha$. Near-coincidence sites (NCS) [15] are employed to highlight the distribution of misfit. The threshold of the NCS is 15% of a_α, since a_α is the smallest α-lattice distance. The matching state of interpenetrating τ and α lattices projected along **z** axis is shown in Fig. 2a within a region of 60 nm × 60 nm. Only the lattice points of the τ phase are drawn for clarity, since the illustrated region is large and